DOI: 10.1364/OE.379512

Research Article | Vol. 28, No. 3 / 3 February 2020 / Optics Express 4258
Optics EXPRESS

High-order dispersion mapping of an optical fiber

A. Gil-Molina,[1,2] J. A. Castañeda,[1,3] D. F. Londono-Giraldo,[5] L. H. Gabrielli,[2] A. M. Cárdenas,[4] and H. L. Fragnito[1,5,*]

[1]Gleb Wataghin Physics Institute, University of Campinas, Campinas – SP, 13083-859, Brazil
[2]School of Electrical and Computer Engineering, University of Campinas, Campinas – SP, 13083-852, Brazil
[3]IPG Submarine Networks Division, Campinas – SP, 13086-902, Brazil
[4]Department of Electronic and Telecommunications Engineering, Universidad de Antioquia, Medellin, Colombia
[5]MackGraphe - Graphene and Nanomaterials Research Center, Mackenzie Presbyterian University, São Paulo – SP, 01302-907, Brazil
*hugo.fragnito@mackenzie.br

Abstract: We report on measurements of high-order dispersion maps of an optical fiber, showing how the ratio between the third and fourth-order dispersion (β_3/β_4) and the zero-dispersion wavelength (λ_0) vary along the length of the fiber. Our method is based on Four-Wave Mixing between short pulses derived from an incoherent pump and a weak laser. We find that the variations in the ratio β_3/β_4 are correlated to those in λ_0. We present also numerical calculations to illustrate the limits on the spatial resolution of the method. Due to the good accuracy in measuring λ_0 and β_3/β_4 (10^{-3}% and 5% relative error, respectively), and its simplicity, the method can be used to identify fiber segments of good uniformity, suitable to build nonlinear optical devices such as parametric amplifiers and frequency comb generators.

1. Introduction

It is well known that optical fibers exhibit random longitudinal variations of their chromatic dispersion properties, resulting from the drawing and preform fabrication processes [1–3]. These fluctuations are a shortcoming on the efficiency of parametric devices based on Four-wave mixing (FWM), especially fiber optical parametric amplifiers (FOPAs) [3–6]. In most studies, the influence of dispersion fluctuations on the FOPA gain has been evaluated in terms of the variations of the zero-dispersion wavelength (λ_0) or the wavevector mismatch ($\Delta\beta$). A more complete analysis should consider also the fluctuations of high-order dispersion (HOD) (i.e. $\beta_n = d^n\beta(\omega)/d\omega^n|_{\omega=\omega_0}$, for $n > 2$), given that minute changes in HOD have a strong impact in FWM-based parametric devices [7–17]. HOD is also important in fiber solitons and supercontinuum generation [17–22]; and ultra-high-capacity optical communications, in which the compensation of residual dispersion up to fourth-order is required [23–25]. Accurate modeling in all these problems require knowledge of the HOD dispersion maps.

Given that FWM is very sensitive to dispersion, several dispersion characterization methods based on FWM have been experimentally demonstrated in optical fibers [26–43]. Some of these methods provide useful information about dispersion fluctuations along the fiber length, also known as dispersion mapping techniques [34–43]. The first dispersion mapping experiment was presented by Honaka et al. [34], in which a map of λ_0, i.e. $\lambda_0(z)$, was obtained by cutting a 23 km dispersion shifted fiber (DSF) in segments from 0.3 to 1 km, and fitting the measured FWM conversion efficiency spectrum of each segment with a theoretical prediction. Since then,

#379512 https://doi.org/10.1364/OE.379512
Journal © 2020 Received 9 Oct 2019; revised 8 Dec 2019; accepted 9 Dec 2019; published 31 Jan 2020

Optics EXPRESS

many non-destructive dispersion mapping techniques have been demonstrated [35–43] that may be classified as follows:

Type I methods measure the FWM conversion efficiency [35,36] or the parametric gain spectrum [37] generated by continuous wave (CW) tunable lasers, at the output of the fiber, as a function of wavelength (and keeping a constant wavelength difference between the two lasers). In the end, a numerical approach is used to retrieve $\lambda_0(z)$ by fitting.

Type II methods measure the FWM spectrum generated by two overlapping pulses [38,39]. One of the pulses (used as a pump) is tuned around λ_0, and the second pulse (used as a signal) is located far from λ_0 (~80 nm). Because of the difference in group velocities, both pulses overlap just along a specific segment of the fiber. The FWM efficiency as a function of the signal frequency exhibits a maximum when the phase-matching condition is satisfied (i.e. $\Delta\beta = 0$), which is used to obtain λ_0. Then $\lambda_0(z)$ is obtained by varying the spatial overlap region along the entire fiber by adjusting the initial delay between the pulses. If the overlap region is longer than the correlation length of the dispersion fluctuations, the so measured FWM spectrum may exhibit more than one maximum, indicating that there is more than one λ_0 within that particular fiber segment [38]. The shortest overlap region obtained in DSFs is ~700 m by using ~100 ps pulses [39]. A better spatial resolution can be obtained by using shorter pulses, but at the expense of a coarser spectral resolution [38,39].

Type III methods measure the Rayleigh backscattered power of a wave parametrically amplified [40] or generated [41] by FWM, by means of an optical time-domain reflectometry (OTDR) configuration. In [40], the $\lambda_0(z)$ map is obtained by identifying the transition between normal and anomalous dispersion, tuning a pump laser around λ_0 and measuring the OTDR trace at a probe wavelength, considering that there is an abrupt increase in this backscattered power when the pump wavelength matches λ_0. In [41], the chromatic dispersion map $D(z)$ is obtained by using two lasers and measuring the backscattered power at one of the generated FWM frequencies. This OTDR trace oscillates locally with a spatial period related to $D(z)$. Despite the ease of implementation, these OTDR-based methods have limited spatial resolution (~1 km), which is associated to the OTDR sensitivity requirements. For instance, the spatial resolution in [40] could be improved by reducing the width of the probe pulse, but at the expense of a reduced OTDR signal. Similarly, in [41] the spatial resolution could be improved by increasing the separation of the FWM pump lasers, but this would result again in a weaker OTDR signal [42].

Type IV methods measure either $D(z)$ [42] or $\lambda_0(z)$ [43] from the spatial oscillations of the FWM power generated with two pump lasers and exploit the strength of stimulated Brillouin scattering (SBS), to amplify the FWM signal instead of the weak Rayleigh backscattering. Thus, overcoming the sensitivity and spatial resolution limitations of Type III methods. In [42], a counter propagating pump pulse provides a local SBS gain to the spatially oscillating FWM, which is detected in transmission by optical filtering (instead of back reflection). Thus, the $D(z)$ map is obtained with a spatial resolution of ~ 20 m for standard single-mode fibers (SMFs) and ~ 150 m for DSFs. In [43], an enhanced configuration uses FWM and SBS pulsed pumps and, therefore, the detected FWM power is generated only from the short overlap region between the counter-colliding pulses, achieving a meter-scale spatial resolution. Subsequently, the $\lambda_0(z)$ map is retrieved by means of processing the detected raw data. In this method, the spatial resolution is limited by the width of the SBS pump pulse (~25 ns due to the SBS bandwidth). However, an even better resolution (10 μm) could be achieved by using stimulated Raman scattering gain mechanism [43].

A common characteristic between all mentioned dispersion mapping experiments is that the effect of HOD is either neglected or assumed to be constant along the optical fiber. In addition, although some FWM-based dispersion characterization methods are capable of measuring the average λ_0 and HOD parameters [30–32], they have not been implemented as dispersion mapping

Optics EXPRESS

techniques. Moreover, most of the methods require significant data treatment to retrieve the dispersion map from the raw data and/or complex experimental setups.

In this paper, we present a new high-order dispersion mapping method based on [31,32], which allows the measurement of longitudinal fluctuations of λ_0 and the ratio between the third and fourth-order dispersion parameters (i.e. β_3/β_4). Our measuring method uses a time of flight concept as in type II, as it is based on the FWM interaction between two overlapping pulses. However, one of the pulses is from an incoherent pump source and the other is from a weak laser. The use of an incoherent pump instead of a pump laser presents several advantages [31,32]. First, the time-consuming process of tuning the wavelength of the pump around λ_0 is no longer needed, given that the incoherent pump contains all the necessary Fourier components to drive the complete FWM spectrum in a single shot. Second, a single measurement of the FWM spectrum allows to visualize the uniformity of the chromatic dispersion of the overlap segment [44]. Third, the large bandwidth of the incoherent pump prevents SBS, which usually limits the pump power in other dispersion-mapping techniques.

We present measured maps of λ_0 and β_3/β_4 in a 7 km DSF, and show that the variations of these dispersion parameters are correlated. We also evaluate the fiber dispersion by using a numerical model of a multi-layered step-index fiber profile [45], showing that the measured dispersion fluctuations may be explained in terms of geometrical variations along the fiber.

The rest of the paper is organized as follows: In section 2 we present the measuring principle of dispersion mapping by using incoherent-pulsed-pumped FWM; in section 3 we describe our experiments; in section 4 we show our experimental results; and in section 5 we discuss the spatial resolution of our method, and the possible physical origins of the dispersion fluctuations. Finally, we draw our conclusions in section 6.

2. Dispersion mapping by using incoherent-pulsed-pumped Four-Wave Mixing

Our method consists in measuring the power spectrum generated by FWM between an incoherent pump centered close to λ_0, and a weak laser tuned far from λ_0 [31,32]. This type of FWM can be treated analytically in the frequency domain. With some approximations and assumptions on the nature of the stochastic field, we can predict the shape of the FWM spectrum and how it depends on experimental parameters such as the laser frequency and fiber length. A more accurate description is discussed at the end of this section.

We consider a non-uniform single-mode fiber, whose dispersion parameters vary along its length, but we restrict our attention to the case where the variations are sufficiently small that the mode profile is unperturbed. In this case, we can represent the (positive frequency) Fourier amplitude of an optical field as $A(z,\nu)e^{i\bar{\beta}z}$, where $\bar{\beta} = \int_0^z \beta(z',\nu)dz'/z$ is the cumulative moving average of the propagation constant, and A is an amplitude that varies slowly in space. We can use the equations written for the case of uniform fibers and CW sources [31] by substituting β with $\bar{\beta}$ (and taking due care, since $\bar{\beta}$ is function of z). Thus, the FWM spectral field (A_{FWM}) generated in a fiber segment between z_1 and z_2, can be written as

$$A_{FWM}(\nu) = i\gamma E_\ell^* \int A_1 A_2 f(\nu,\nu_1)d\nu_1, \tag{1}$$

where

$$f(\nu,\nu_1) = \int_{z_1}^{z_2} e^{i\Delta\bar{\beta}z}dz. \tag{2}$$

Here γ is the nonlinear coefficient, the laser has been considered as $A(\nu) = E_\ell\delta(\nu-\nu_\ell)$; $A_1 = A(\nu_1)$ and $A_2 = A(\nu_2)$ correspond to two Fourier components, respectively at frequencies ν_1 and $\nu_2 = \nu + \nu_\ell - \nu_1$ within the incoherent spectrum, which is centered at ν_p and has width $\Delta\nu_p \ll |\nu_p - \nu_\ell|$. Finally, $\Delta\bar{\beta} = \bar{\beta}(\nu) + \bar{\beta}(\nu_\ell) - \bar{\beta}(\nu_1) - \bar{\beta}(\nu_2)$ is the relevant propagation constant mismatch. In Eq. (1) we have neglected the fiber loss (i.e., the attenuation coefficient $\alpha = 0$) as

Optics EXPRESS

well as pump depletion, self-phase and cross-phase modulation, and assumed that the pump and laser fields are linearly polarized in the same direction (scalar approximation).

The FWM power spectrum can be obtained from Eq. (1) by taking into account the statistical properties of the incoherent source [46,47], which is assumed to satisfy

$$\langle A(\nu')A^*(\nu)\rangle = S(\nu)\delta(\nu'-\nu), \text{ and} \tag{3a}$$

$$\left\langle A_1'A_2'A_1^*A_2^*\right\rangle = \left\langle A_1'A_1^*\right\rangle\left\langle A_2'A_2^*\right\rangle + \left\langle A_1'A_2^*\right\rangle\left\langle A_2'A_1^*\right\rangle$$

,where $S(\nu)$ is the power spectral density (W/Hz), $\langle\ \rangle$ stands for statistical average, and $A_k{}' = A(\nu_k{}')$. These relations are valid for circular Gaussian processes and are very plausible for the source used in our experiment. The FWM spectrum $\left\langle A_{FWM}(\nu')A_{FWM}^*(\nu)\right\rangle = S_{FWM}(\nu)\delta(\nu'-\nu)$ is then expressed as

$$S_{FWM}(\nu) = 2\gamma^2 P_\ell \int S(\nu_1)S(\nu_2)|f(\nu,\nu_1)|^2 d\nu_1, \tag{4}$$

where P_ℓ is the laser power. In a uniform fiber, $S_{FWM}(\nu)$ is maximum at a frequency ν_{FWM}, such that the phase-matching condition of the FWM process is satisfied ($\Delta\beta = 0$). Neglecting fifth and higher order dispersion we can express this condition as

$$\frac{\beta_4}{12}(\omega_c-\omega_\ell)^2 = -\left[\beta_3(\omega_c-\omega_0)+\frac{\beta_4}{2}(\omega_c-\omega_0)^2\right], \tag{5}$$

where $\omega_c = (\omega_{FWM}+\omega_\ell)/2$. It is possible to show that the FWM peak is maximized if $\omega_p = \omega_c$.

From Eq. (5) we can obtain ω_{FWM} as a function of ω_ℓ. This dependence is then used to fit the measured peak position ω_{FWM}, as we tune ω_ℓ over a range of frequencies and, therefore, retrieve ω_0 and β_3/β_4 as fitting parameters. Note that we do not fit the spectral shape, but only the peak position.

It can be shown that for ν around the FWM peak, $|f(\nu,\nu_1)|^2$ is a very smooth function of ν_1 and can be taken outside the integral symbol in Eq. (4), with its value at $\nu_1 = \nu_p = \nu_c$. The FWM spectrum is then

$$S_{FWM}(\nu) = 2\gamma^2 P_\ell |f(\nu,\nu_c)|^2 \int S(\nu_1)S(\nu+\nu_\ell-\nu_1)d\nu_1. \tag{6}$$

The remaining integral in Eq. (6) is the autoconvolution of the pump spectral power density and is weakly dependent on ν. Therefore, the spectral shape of the FWM field is essentially given by the function $|f(\nu,\nu_c)|^2$. Although Eq. (2) shows how this function depends on $\Delta\beta$, this also gives the dependence with frequency since, around the FWM peak, $\Delta\beta$ is approximately proportional to $\Omega = \omega - \omega_{FWM}$: $\Delta\beta \approx b\Omega$, with the coefficient $b = \beta_3(\omega_{FWM}-\omega_\ell)^2/8$.

Equation (6) applies for the case of CW sources. In the experiments reported here we use short light pulses that superpose over a limited region of fiber. This region is centered at a crossing position z_x and has a length $2\,\sigma_z$ (often called the interaction or walk-off length). We control z_x by varying the delay (τ) between the pump and the laser pulses. We can estimate the measured spectrum by using Eq. (6) (with an appropriate duty cycle factor) but with the integral in Eq. (2) taken over the region where the pulses overlap. At this point it is perhaps instructive to look at the animation in Visualization 1, where we show how the FWM spectrum is generated as the pulses cross in different positions.

The interaction length can be estimated crudely as $\delta t/|\delta\beta_1|$, where $\delta\beta_1 = \beta_1(\omega_\ell) - \beta_1(\omega_p)$ is the group delay difference ($v_g = 1/\beta_1$ is the group velocity), and δt is the time required for the fastest pulse (the pump in our experiments) to pass through the slower pulse and having significant power to generate measurable amounts of FWM. A more precise approach is as follows [39]: we introduce an overlap function that takes into account the envelope functions a_ℓ and a_p of the laser and pump fields in the time domain, $g(z) = \int_{-\infty}^{\infty} a_\ell(t)a_p^2(t-\tau+\delta\beta_1 z)dt$, which for the case of

Optics EXPRESS

Gaussian pulses with RMS widths σ_ℓ and σ_p, we obtain $g(z) = \exp[-(z - z_x)^2(2\sigma_z)^{-2}]$, i.e., a Gaussian centered at $z_x = \tau/\delta\bar{\beta}_1$, and with variance $\sigma_z^2 = (\sigma_\ell^2 + \sigma_p^2/2)/(\delta\beta_1)^2$. This function is used to redefine f in Eq. (2) as

$$f(\nu, \nu_c) = \int_0^L g(z) e^{i\Delta\bar{\beta}z} dz \tag{7}$$

The integration is now over the whole fiber, since the relevant segment of fiber is automatically selected by the overlap function. If we divide the fiber into segments of uniform dispersion and lengths L_1, $L_2 \ldots$, we can estimate the FWM spectrum from a particular segment L_k by considering the integral in Eq. (7) just over this segment, f_k. There are two interesting limits: If $L_k \ll 2\sigma_z$, then we can set $g(z) \approx 1$ in Eq. (7), with the result that $|f_k|^2 = L_k^2 \mathrm{sinc}^2(\Delta\beta_k L_k/2)$, where $\mathrm{sinc}(x) = \sin(x)/x$. The spectrum then shows a central peak of width (full-width at half-maximum, FWHM) $\Delta\Omega \approx 2\pi/(b_k L_k)$ [32], and sidelobes typical of the sinc^2 function. However, in this case, the overlap function covers at least partially one or two adjacent segments, and the FWM light from these last will interfere with that from L_k, giving a structured spectrum. In the other extreme, if $L_k \gg 2\sigma_z$, we can extend the limits of integration in Eq. (7) to $\pm\infty$, and f_k becomes just the spatial Fourier transform of $g(z)$: $|f_k|^2 = 4\pi\sigma_z^2 \mathrm{e}^{-2\Delta\beta_k^2\sigma_z^2}$. In this case, the FWM spectrum is a narrow Gaussian, with FWHM width $\Delta\Omega \approx \sqrt{2\ln(2)}/b_k\sigma_z$. Examples of these cases will be shown in Section 5. In practice, thus, we take the interaction length as $2\sigma_z$ and estimate this quantity directly from the width of the FWM spectrum corresponding to the most uniform segment, where a single, narrow peak is observed.

The above analysis is useful to provide insights on this incoherently pumped FWM process. We have neglected several effects that deserve comments. Fiber loss and pump depletion can be introduced by an effective loss factor $e^{-\alpha z}$ inside the integral in Eq. (7). This tends to decrease the contrast of the sidelobes of the sinc^2 type spectra. In this same direction, the presence of spatially fast fluctuations can be treated with an extra loss coefficient [48]. Dispersion broadening of the pulse envelopes are small because the laser is bandwidth limited and the pump is very close to the zero-dispersion wavelength. A small pulse broadening effect lowers the pulse peak powers, but is partially compensated by the concomitant lengthening of the overlap region. None of these effects shifts the position of the FWM peak. Nonlinear phase modulation, on the other hand, do shift the spectrum and imposes a limit on the amount of pump power that can be used in the experiments. In practice, one should always verify that the FWM peak does not vary by reducing the pump power. Finally, the validity of Eqs. (3a) and (3b) may be questioned, since the field of a pump pulse is not a stationary random process. We can say here that, in the experiments, the pulses are produced by using an electro-optical modulator at hundreds of MHz, thus these pulses are samples of an originally true stationary process and the optical spectrum analyzer instrument (whose response time is of the order of tens of milliseconds or larger) takes averages over millions of pulses. For such large number of samples, the statistical relations in (3a) and (3b) are expected to be the same as those of the original stationary process.

For a more realistic calculation of the spectral shape, we solve a generalized scalar generalized Nonlinear Schrodinger Equation (NLSE) taking into account high order dispersion and its longitudinal variation, the measured pulse shapes, the fiber loss, and a randomly generated field for the incoherent source. The most relevant nonlinear effects (FWM, Self and Cross Phase Modulation, Modulation Instability and cascaded effects) are well accounted for with this approach. However, these simulations are time consuming due to the randomness of the process and the short duration of the pulses. For short pulses, we are essentially sampling the stationary process during a very short time, and thus we require averaging over hundreds of realizations to obtain a stable spectrum. Results from these simulations are presented later in sections 4 and 5.

Optics EXPRESS

3. Experiments

Our experimental setup is presented in Fig. 1. The interacting incoherent-pump and laser pulses were generated at the pump and laser stages, respectively.

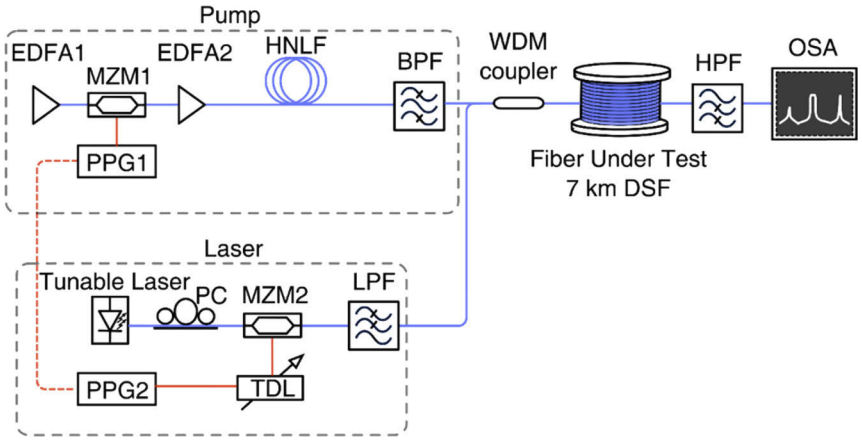

Fig. 1. Dispersion-mapping experimental setup: EDFA, erbium-doped fiber amplifier; MZM, Mach-Zehnder modulator; PPG, pulse pattern generator; PC, polarization controller; TDL, time delay line; HNLF, highly-nonlinear fiber; BPF, optical bandpass filter; WDM, wavelength division multiplexer; DSF, dispersion shifted fiber; HPF, optical high-pass filter; LPF, optical low-pass filter; OSA, optical spectrum analyzer.

We derived the pump from a spectrally sliced supercontinuum, due to the fact that we wanted to explore different pump regions, not limited by that of the amplified spontaneous emission (ASE) of the available erbium-doped fiber amplifiers (EDFAs) in our laboratory. The supercontinuum was generated in 38 m of HNLF (nonlinear coefficient $\gamma \approx 6$ W^{-1} km^{-1} and $\lambda_0 \approx 1554$ nm), seeded by a high peak power pulsed ASE (~10 W of peak power measured with a 28 GHz bandwidth photodetector), and then spectrally sliced by using an optical bandpass filter (BPF). This BPF consisted of a fiber connectorized monochromator (*Yenista WSM-160*), tunable both in bandwidth (from 0.25 to 60 nm) and in central wavelength (from 1510 to 1635 nm). In order to obtain the pulsed ASE, the ASE from EDFA1 was intensity-modulated by using a Mach-Zehnder modulator (MZM1), driven by a pulse train of ~ 25 ps duration (FWHM) and 155 MHz repetition rate, generated by a pulse pattern generator (PPG1). Subsequently, a second amplifier (EDFA2) was used to boost the power of the pulsed ASE.

The laser, on the other hand, consisted of a tunable laser intensity-modulated by MZM2 (both MZM1 and MZM2 have $\gtrsim$ 30 dB extinction ratio and 20 GHz bandwidth), driven by ~35 ps duration pulses at 155 MHz, generated by PPG2 (synchronous to PPG1). Subsequently, the laser pulses were passed through an optical low-pass filter (LPF, *AC Photonics MWDM 54*, with cutoff wavelength of 1510 nm and an out-of-band rejection >20 dB) in order to reject the laser noise at the expected wavelength region for the FWM spectrum (i.e. between 1472 and 1493 nm).

The pump and laser pulses were coupled into the FUT by using a wavelength division multiplexer (WDM) coupler. The FUT consisted in a DSF of 7 km (Corning) with $\lambda_0 \approx 1550.8$ nm, as previously measured by using a dispersion measuring instrument (*2008 Chromatic Dispersion Measurement System, by Photon Kinetics*) and $\gamma \approx 2.3$ W^{-1}km^{-1} [26]. We have chosen a DSF as our FUT because almost all the equipment available in our laboratory operates around 1550 nm (i.e. amplifiers, modulators, lasers). Obviously, the method can be applied to other fibers with proper equipment. Figures 2(a) and 2(b) show the pump and laser pulses at the input of the FUT with a peak power of ~200 and ~2 mW respectively. Although the electrical

Optics EXPRESS

pulses from the PPGs had 25 ps and 35 ps of FWHM for the pump and laser respectively, the optical pulse measured durations were 39 ps and 43 ps. This difference can be attributed to the limited bandwidth of the MZMs (20 GHz).

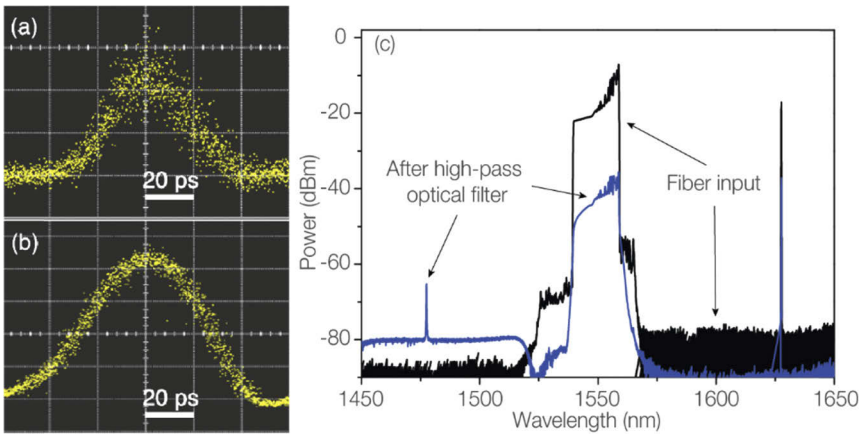

Fig. 2. Temporal and spectral characteristics of the experiments: (a) Pump and (b) laser pulses at the input of the FUT (measured by an oscilloscope with a 28 GHz built-in detector). (c) Optical spectrum at the input of the FUT and at the output, after the high-pass optical filter. Both spectra were measured with λ_ℓ = 1627.56 nm and a resolution bandwidth of 100 pm.

We placed the fiber inside a box to minimize dispersion changes due to temperature variations (ΔT). Since $d\lambda_0/dT$ in DSFs is ~ 0.03 nm/°C [49], we ensured that $\Delta T < 1$ °C inside the box.

Figure 2(c) shows the spectrum at the input of the FUT, where the pump has ~17 nm bandwidth, and at the output, but after a high-pass optical filter (HPF) used to attenuate the laser and the pump. This filter (*AC Photonics MWDM 54*, cutoff wavelength of ~1510 nm and an out-of-band rejection of ~25 dB) significantly reduces the background level which is due stray light within the OSA. The output spectrum, so filtered, exhibits a FWM peak generated with ~15 dB of signal to noise ratio (SNR).

The overlap region between the pulses was controlled by means of a time delay line (TDL, *Narda Microwave RF phase shifter*) after the pulse pattern generator PPG2, which triggers PPG1. For each laser wavelength, we measured the FWM power spectrum for 58 different delays between both pulses at the input of the FUT, thus, each delay step corresponded to a fiber step size of $\Delta L \approx 120$ m. We verified that no FWM was generated when the pulses overlapped outside the FUT, and that at the 155 MHz repetition rate, the pulses overlapped only once in the FUT.

We measured the FWM power spectrum for all delays at five different laser wavelengths (i.e. λ_ℓ = 1610.54, 1616.54, 1622.56, 1627.56 and 1632.54 nm). For each delay, we used the measured set of ω_{FWM} for the five values of ω_ℓ, and then fitted the relations between ω_ℓ and ω_{FWM} described in Section 2. The measured values of λ_0 and β_3/β_4 that were obtained as fitting parameters were used to construct the dispersion maps (see Results). An important point must be considered regarding the use of pulses for the construction of dispersion maps, is the fact that, for different laser wavelengths, the same value of the delay does not correspond to the same overlap region in the fiber, since the group-delay depends on wavelength. One should take into account this dependence when selecting the delay step.

Optics EXPRESS

4. Results

In Fig. 3, we show the normalized FWM power spectrum generated in a DSF of 7 km by using CW sources [Fig. 3(a)] and by using pulses [Fig. 3(b)] with the delay adjusted to superpose the pulses in four different fiber segments. Comparing the FWM power spectra generated by CW and pulsed sources, one can note that each FWM peak that appears in the CW spectrum can be spatially resolved. In both cases (CW and pulses), the pump source is the same, since the pump pulses are obtained from the CW source that has been passed through an electrooptic modulator, thus the pulses can be seen as temporal samples (of ~40 ps duration) of an otherwise stationary random field.

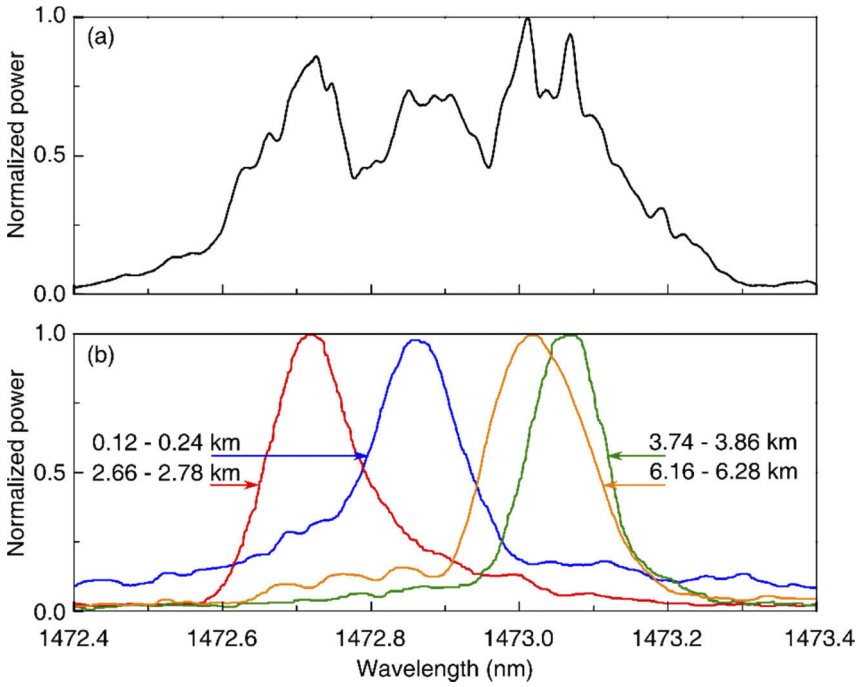

Fig. 3. Normalized FWM power spectra generated by an incoherent pump and a comparatively weak laser (at $\lambda_\ell = 1632.54$ nm): (a) CW sources; (b) pulsed sources with a relative delay adjusted to superimpose the pulses at four different segments of the same fiber. All spectra were measured with a resolution bandwidth of 10 pm.

We now present the measured maps for λ_0 and β_3/β_4 in Figs. 4(a) and 4(b), respectively. Our measured maps reveal that λ_0 varies around a mean value $\lambda_0 \approx 1550.5$ nm with a standard deviation of $\sigma(\lambda_0) \approx 0.1$ nm. Meanwhile, β_3/β_4 varies around $\beta_3/\beta_4 \approx -220$ ps^{-1} with $\sigma(\beta_3/\beta_4) \approx -10$ ps^{-1}. The standard deviation of each data point [indicated by the vertical width of the shadowed areas in Figs. 4(a) and 4(b)] was estimated assuming that λ_ℓ and λ_{FWM} were measured with an uncertainty of 0.1 nm, which corresponds to a typical wavelength shift of the OSA when not calibrated. However, we have verified the calibration of the OSA before and after every set of measurements, thus, the shadowed areas in Fig. 4 are somewhat overestimated. We have also made two important verifications. First, we have verified that λ_{FWM} did not shift with the pump power, thus, ensuring that the phase-matching condition was power independent. Second, we have verified that varying the state of polarization of the laser relative to that of the pump (by means of another PC, not shown in Fig. 1) did not cause a shift of the FWM spectrum. We also

Optics EXPRESS

point out that in the CW case we can excite the fiber with an unpolarized pump source, and the measured FWM spectrum does not differ from that reported in Fig. 3(a).

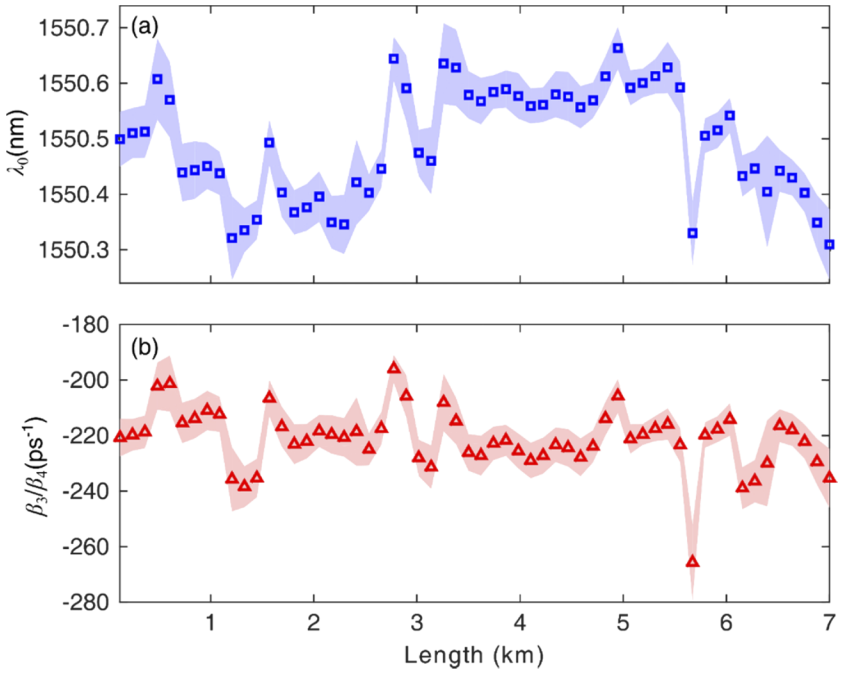

Fig. 4. Maps for (a) λ_0 and (b) β_3/β_4. The symbols (squares and triangles) represent the measured mean values and the measured standard deviations are represented by the shadowed areas.

One can see from Fig. 4 that the maps show some correlation between the measured dispersion parameters λ_0 and β_3/β_4. These maps also show that the measured fiber has two regions with larger variations, i.e. from 0 to 3.5 km and from 5.5 to 7 km. In contrast, the region between 3.5 and 5.5 km seems to be more uniform. This region would be suitable, for example, to build efficient parametric devices such as amplifiers or wavelength converters.

A clear evidence of the longitudinal fluctuations of $\Delta\beta$ is the evolution of the measured FWM power spectrum along the fiber, as it is shown in Fig. 5(a) for $\lambda_\ell = 1632.54$ nm (normalized to the peak power). In order to further support the validity of our measured maps shown in Fig. 4, we included in Fig. 5(b) the calculated FWM power spectrum using incoherent-pump and laser pulses with similar power and temporal and spectral characteristics as those used in our experiments. For the numerical calculations we solved the generalized NLSE by means of a split-step Fourier method (SSFM) [50] along 58 concatenated fibers, each with ~120 m of length, and $\lambda_0(z)$ corresponding to the measured zero-dispersion wavelength map in Fig. 4(a). Our calculations of fiber dispersion (see Section 5.2) and measurements in two similar fibers show that β_3 is more affected by fiber non-uniformities than β_4. Therefore, for the simulations we assumed a constant $\beta_4(z) = \beta_4 = \beta_3/\beta_3/\beta_4 = -5.6 \times 10^{-4}$ ps^4/km (considering the measured $\beta_3 = 0.123$ ps^3/km by using a dispersion measuring instrument) and a longitudinal variation of $\beta_3(z) = \beta_4 \frac{\beta_3}{\beta_4}(z)$ given by the measured β_3/β_4 map in Fig. 4(b). As shown in Figs. 5(a) and 5(b), our calculations are in good agreement with our experiments.

Optics EXPRESS

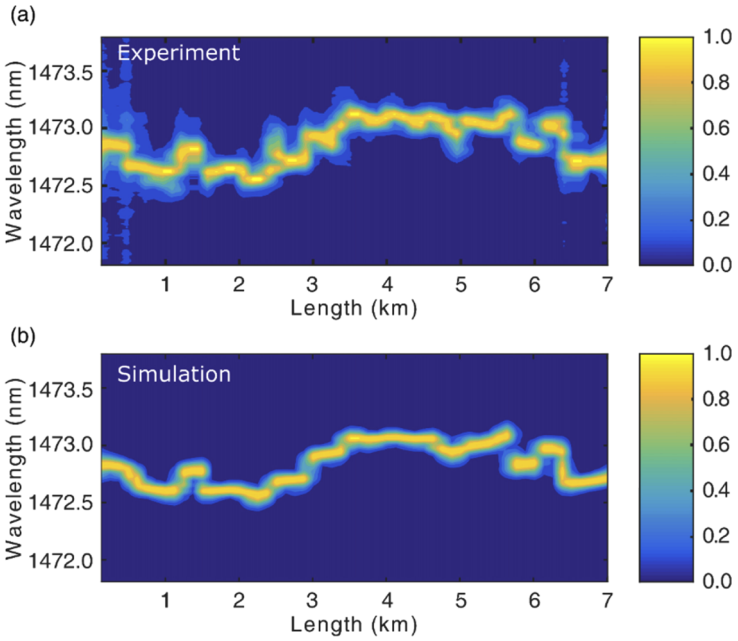

Fig. 5. Normalized FWM power spectrum along the fiber length with $\lambda_\ell = 1632.54$ nm. (a) Measured spectra with a resolution bandwidth of 10 pm. (b) Simulated spectra using the generalized NLSE (each spectrum is averaged over 100 realizations).

5. Discussion

5.1. Spatial resolution and sensitivity

As mentioned before, the spatial resolution of type II methods has been attributed to the walk-off length [38,39] that for pulses of 40 ps of FWHM in our fiber gives $2\sigma_z \approx 200$ m. However, our experiments (made with a step size $\Delta L \approx 120$ m) show abrupt variations of λ_{FWM}, which indicate that a better resolution should be possible [see Fig. 5(a)].

In general, the spatial resolution depends on the pulse duration, dispersion of the sources, and step size. Also, as in all OTDR type of measurements, a trustable value of the group velocity is necessary to translate time measurements into absolute distance along the fiber. Given that our dispersion maps were elaborated by identifying the transition of λ_{FWM} (as illustrated in Fig. 5), two important questions arise: (*i*) What is the minimum uncertainty ΔL that allows to localize the position where a transition in λ_{FWM} occurs? (*ii*) What is the minimum length of a fiber segment with uniform dispersion but different from the surrounding fiber that can produce a detectable FWM peak? We address these questions by means of simulation of two scenarios.

The first scenario, schematized in Fig. 6(a), corresponds to an ideal case of two consecutive uniform fibers with different zero-dispersion wavelengths, namely $\lambda_0 = 1550.55$ and 1550.45 nm for the first and second fiber respectively, whereas HOD is the same in both fibers (i.e., $\beta_3 = 0.123$ ps^3/km and $\beta_4 = -5.6\times10^{-4}$ ps^4/km). For this simulation, we have used similar pulses as those used in our experiments (i.e., FWHM pulse duration of ~ 39 ps and ~ 43 ps, respectively, for the pump and the laser) and calculated the FWM power spectrum along the fibers by changing the initial delay between pulses (τ), as we did experimentally, but using a finer step size of $\Delta L \approx 45$ m (corresponding to a delay step of ~ 10 ps). Each spectrum was calculated 200 times to obtain a stable peak. In this scenario, two FWM spectral peaks can be identified and the transition between peaks, represented by a discontinuous line in Fig. 6(a), clearly evidences the change

Optics EXPRESS

of fiber dispersion [see also an animation of the pulses propagation and longitudinal evolution of the FWM power spectrum in Visualization 1]. Furthermore, we have analyzed in detail the transition of power between the two peaks by using an even shorter step size of $\Delta L \approx 2.25$ m in our calculations (i.e., delay step of ~ 0.5 ps). We show this transition in Fig. 6(b) and note that for such a small change in the crossing position of the pulses a relative power difference of ~5% between the two FWM peaks is produced. Similarly, we have calculated that a relative power difference of ~2% between the two FWM peaks (i.e., ~ 0.1 dB) could be identified when using a $\Delta L \approx 0.90$ m (equivalent to a delay step of ~ 0.2 ps). Therefore, considering that power changes of 0.1 dB are detectable by means of a commercial OSA (as the one used in our experiments), a step size of $\Delta L \approx 0.9$ m could be considered as the limit in localizing transitions of fiber dispersion. In addition, we have evaluated the same scenario by using broader pulses of ~ 100 ps FWHM width and found that the limit in localizing dispersion transitions (~2% relative power difference between two peaks) is $\Delta L \approx 3$ m.

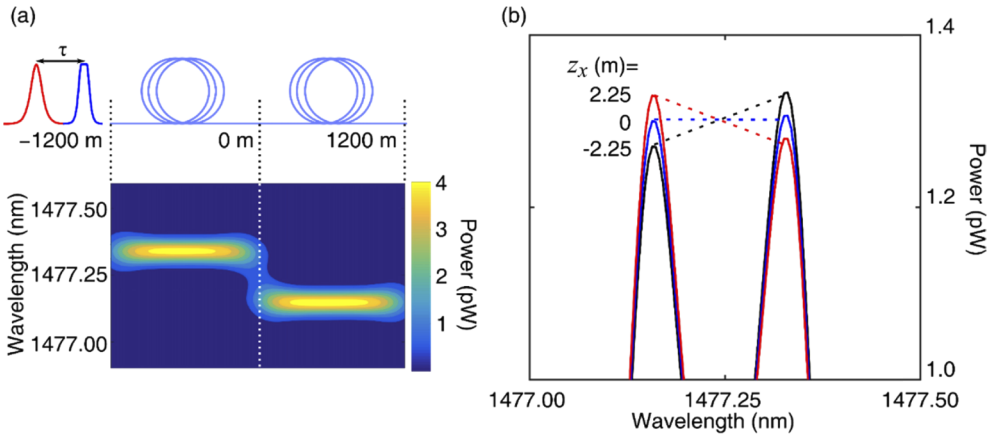

Fig. 6. Simulation scenario of two consecutive fibers with different λ_0 (1550.55 and 1550.45 nm), same HOD parameters (β_3 = 0.123 ps^3/km and β_4 = –5.6×10^{-4} ps^4/km) and λ_ℓ = 1627.6 nm. (a) calculated FWM power spectrum along the fibers in steps of $\Delta L \approx 45$ m. (b) Power transition between FWM peaks in steps of $\Delta L \approx 2.25$ m. Visualization 1 in Supplementary Material shows an animation of the pulses propagation and the evolution of the FWM power spectrum.

In the second scenario we look at the minimum detectable segment where λ_0 is different from the rest. As described in Fig. 7(a) we consider three consecutive fibers, the first and third fibers are identical, with λ_0 = 1550.65 nm, whereas the second fiber has λ_0 = 1550.35 nm (HOD parameters were kept constant in all three fibers, β_3 = 0.123 ps^3/km and β_4 = – 5.6×10^{-4} ps^4/km). The lengths of the first and third fibers were $L_1 = L_3 = (L - L_2)/2$, with a fixed total L = 1200 m, whereas the length of the second fiber (L_2) was varied. In Fig. 7(b) we show the generated FWM power spectrum for three different values of L_2 and the delay such that the crossing position of the pulses is at the midpoint of the concatenated fibers (i.e., $z_x = L_1 + L_2/2 = L/2$).

In the case of long L_2 [900 m in Fig. 7(b)], the corresponding FWM peak can be easily identified and, as expected, has more power than that corresponding to L_1 and L_3. In addition, as explained in Section 2, the FWM peak from L_2 represents a clear example of the case where the length of the uniform fiber is longer than the interaction length of the pulses (i.e., $L_2 \gg 2\sigma_z \approx$ 200 m). Thus, according to the arguments in section 2, the FWM spectral shape from the central segment is a narrow Gaussian. In contrast, the FWM peak at a longer wavelength resembles the sinc^2 type of spectrum, corresponding to a short length of fiber (arising from the partial overlap

Optics EXPRESS

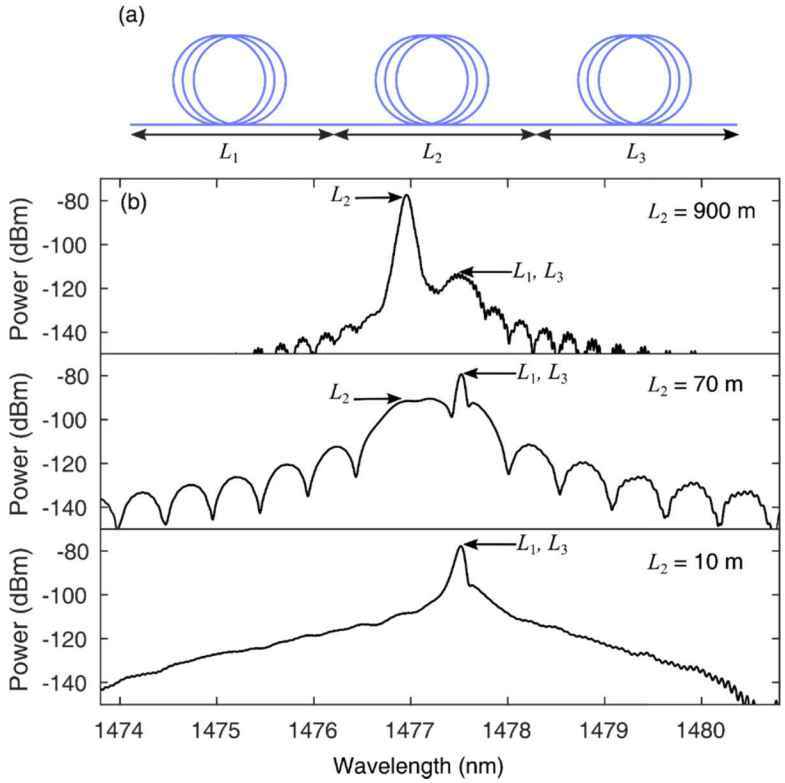

Fig. 7. Simulation scenario of three consecutive fibers. (a) The first and third fibers are identical, with λ_0 = 1550.65 nm, and the second fiber has λ_0 = 1550.35 nm (HOD parameters β_3 = 0.123 ps^3/km and β_4 = –5.6×10^{-4} ps^4/km were kept constant in all fibers). (b) Calculated FWM power spectrum (with λ_ℓ = 1627.6 nm) for different values of L_2.

of the pulses along the end region of L_1 and the beginning region of L_3, adding up to a length that is shorter than $2\sigma_z$).

In the case of shorter L_2 [70 m in Fig. 7(b)], the corresponding FWM peak is comparatively broader and smaller in height, but the two FWM peaks can still be identified. In addition, the Gaussian and sinc^2 spectral shapes of the peaks become inverted in comparison with the previous case of 900 m. This is due to the fact that the pulse overlap takes place mostly along fibers L_1 and L_3.

In the case of even shorter L_2 [10 m in Fig. 7(b)], the corresponding FWM peak cannot be identified and, therefore, by using our method it is not possible to detect the presence of a such a short segment of fiber.

Although our method can be sensitive enough to localize an abrupt dispersion change within an uncertainty of $\Delta L \approx 0.9$ m, the spatial resolution (in the sense of the shortest segment of fiber that produces a detectable FWM peak) is between 10 and 70 m, depending on the difference between dispersion parameters of the fiber to be detected and those of the adjacent segments, as well as on settable experimental parameters (σ_ℓ , σ_p, and $|\lambda_\ell - \lambda_p|$). We point out that the spatial step in our measured maps ($\Delta L \approx 120$ m) is larger than the estimated limit (~70 m), but still shorter than the pulse's overlap length considering the rms pulse widths, ($2\,\sigma_z \approx 200$ m) – and much shorter than that considering the FWHM pulses widths (470 m). Note also in Fig. 7, that a spurious peak can appear, which is more evident for the 70 m fiber. This is due to interference with the FWM light emitted from adjacent fiber segments [see the discussion following Eq. (7)].

Optics EXPRESS

Experimentally, since the FWM spectrum is continuously displayed in the OSA, one can decide if a given peak is spurious or not by observing its evolution as we vary slightly the delay and/or λ_ℓ.

5.2. Origin of dispersion fluctuations

In order to evaluate possible grounds of the variations observed in our measured maps, we have performed numerical calculations to study how fiber dispersion could be modified by changes in geometry. For the calculations, we assumed the refractive index profile (RIP) shown in Fig. 8(a), which nearly matches the measured RIP of the DSF used in our experiments. In addition, appropriate fiber parameters for our DSF model were found by evaluating λ_0 and β_3/β_4 while varying the inner core radius [the base of the inner triangular core in Fig. 8(a)] and the dopant concentration of the core. The dispersion parameters of the obtained DSF model match the measured mean dispersion parameters (i.e. $\lambda_0 \approx 1550.5$ nm and $\beta_3/\beta_4 \approx -220$ ps $^{-1}$). We used a numerical model of a multi-layered step-index fiber profile [45] to calculate $\beta(\omega)$ for a wide frequency range (corresponding to 1330 - 1860 nm), and then, through finite-difference numerical differentiation, we obtained $d^n\beta(\omega)/d\omega^n$. The frequency dependence of the refractive indices of silica and doped-silica glasses have been obtained from Sellmeier formulae [51,52]. The fiber profile was modeled by using different germanium concentrations as dopant for the core and raised-index ring while using Boron as dopant for the cladding.

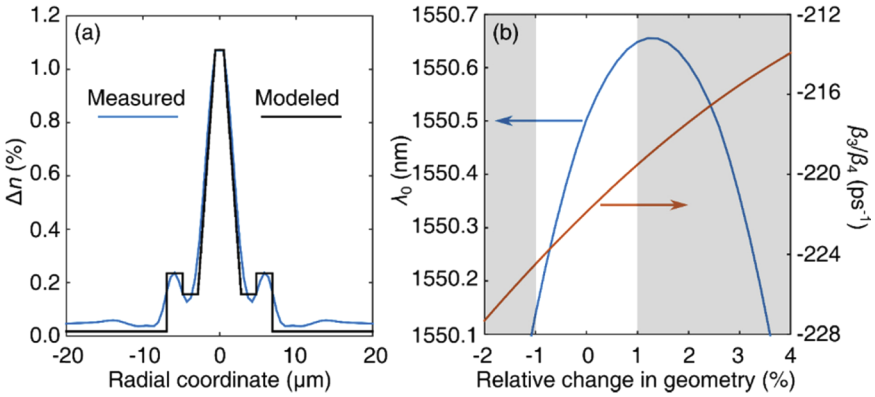

Fig. 8. (a) Measured and modeled refractive index profile at 1550 nm. (b) Calculated λ_0 (left axis) and β_3/β_4 (right axis) as a function of the relative change in fiber geometry.

Given the good agreement between dispersion parameters of the modeled fiber and our measurements, we have evaluated the effect of a uniform 'breathing' of the radial dimensions of the fiber. In Fig. 8(b) we present the calculated variation of λ_0 and β_3/β_4 as a function of this relative change. A variation of λ_0 comparable to that presented in Fig. 4(a) (i.e. approximately from 1550.3 to 1550.7 nm) is observed for a range of relative changes in geometry of the order of ± 1% (this is equivalent to a ± 28 nm change at the base of the core radius). For core radius variations larger than 1%, the variation of λ_0 and β_3/β_4 are no longer correlated, becoming anticorrelated. Meanwhile, for the same relative change in geometry of ±1%, the calculated β_3/β_4 varies about ± 2.5 ps^{-1}. Although, this prediction is comparatively smaller than the range presented in Fig. 4(b), it is worth noting that a variation of ± 2.5 ps^{-1} is within the uncertainty of our method for the measurements of β_3/β_4, which is approximately 7 ps^{-1}.

A uniform deformation, as assumed here, is more likely to be expected in typical preform fabrication and fiber drawing processes, but other non-symmetrical deformations may occur. These last might be invoked to explain the larger variations of β_3/β_4 observed in our FUT. Despite the discrepancy between model and measurements, at least both agree in that the variations in λ_0 and in β_3/β_4 are correlated for geometry variations within ~±1%, as highlighted in Fig. 8(b). We

Optics EXPRESS

should note that other variations in the index profile due to variations in the dopant concentrations and stress should also be taken into account in order to elucidate the physical origin of the high order dispersion fluctuations in fibers.

6. Conclusions

We have experimentally demonstrated high-order dispersion mapping in a DSF of 7 km by means of the FWM interaction between two optical pulses, an incoherent pump and a weak laser.

Although the variation of high-order dispersion has been neglected in previous dispersion mapping experiments, our measurements and numerical calculations show that high-order dispersion exhibits larger variations than λ_0 in this kind of fibers, that is 0.01% in λ_0 and 5% in β_3/β_4. By using a numerical model of an approximate fiber profile, we have explained the observed variations of dispersion in terms of changes in fiber geometry that may arise during fabrication.

Our measurements have revealed a spatial resolution of $\lesssim$120 m, considerably better than that predicted for the walk-off length [38,39] for ~40 ps pulses and relative group delay of $\delta\beta_1 \approx$ 220 ps/km. By using numerical simulations, we have analyzed the main limitations on the spatial resolution of our method and found that it should be possible to localize an abrupt change in λ_0 of ~0.1 nm with a resolution of only ~ 1 m by using delay steps of 200 fs. We also found that the spatial resolution is mostly limited by the fiber length dependence of the FWM power spectrum, which implies that a segment of fiber with uniform dispersion must be long enough ($\gtrsim$ 50 m) to produce a distinguishable FWM spectral peak.

Our method may be useful in several applications, in particular, those that require fibers with uniform dispersion. For example, to build high-performance parametric devices, frequency comb generators, and for experiments sensitive to dispersion such as those found in soliton physics and quantum optics in fibers. By using our method, one should be able to identify the most uniform segments in a long fiber that could be employed to build high performance fiber optical parametric devices.

The high accuracy achieved by our measuring method (i.e. ~40 pm in λ_0 and ~10 ps^{-1} in β_3/β_4) allows it to be applied in special HNLFs or photonic-crystal fibers (PCFs) that are robust against geometry fluctuations [2,53,54]. Our method could be used also with few-mode fibers (FMF) to map not only irregularities, but also the regions where mode coupling occurs. Since the ZDWs of different modes are well separated in typical FMFs, if we want to observe simultaneously the FWM peaks from all modes, we need a sufficiently broadband tunable source, which should be possible by using a supercontinuum source (similar to that used in our experiments). Finally, our method could be a good candidate to evaluate dispersion uniformity of much shorter but highly dispersive waveguides, for example silicon and silicon nitride spirals, by using shorter pulses and larger separation between the laser and the pump wavelengths.

Appendix

Legend to Visualization 1: The left panels represent the pulses propagating along two concatenated fibers for three different initial delays. The right panels show the accumulated FWM spectrum. The pulse parameters are the same as in the experiments, and the fiber parameters are those of Fig. 6. The first (130 ps) and third (390 ps) delays correspond to cases where the pulses overlap on the first and second fiber, respectively. In the case of the second delay (263. 5 ps) the peak of the pulses cross at the transition between the two fibers, generating a spectrum with two peaks of equal heights.

Optics EXPRESS

Funding

Fundação de Amparo à Pesquisa do Estado de São Paulo (2012/50259-8, 2015/11779-4, 2017/16151-9, 2018/08988-9, 2019/16793-6); Coordenação de Aperfeiçoamento de Pessoal de Nível Superior; Departamento Administrativo de Ciencia, Tecnología e Innovación (COLCIENCIAS) (COL-10-2-05).

Disclosures

The authors declare no conflicts of interest.

References

1. N. Kuwaki and M. Ohashi, "Evaluation of longitudinal chromatic dispersion," J. Lightwave Technol. **8**(10), 1476–1481 (1990).
2. M. Hirano, T. Nakanishi, T. Okuno, and M. Onishi, "Silica-based highly nonlinear fibers and their application," IEEE J. Sel. Top. Quantum Electron. **15**(1), 103–113 (2009).
3. M. Karlsson, "Four-wave mixing in fibers with randomly varying zero-dispersion wavelength," J. Opt. Soc. Am. B **15**(8), 2269–2275 (1998).
4. F. Yaman, Q. Lin, S. Radic, and G. P. Agrawal, "Impact of dispersion fluctuations on dual-pump fiber-optic parametric amplifiers," IEEE Photonics Technol. Lett. **16**(5), 1292–1294 (2004).
5. F. Mitra and M. Sterke, "Parametric amplification in presence of dispersion fluctuations," Opt. Express **12**(1), 136–142 (2004).
6. J. S. Y. Chen, S. G. Murdoch, R. Leonhardt, and J. D. Harvey, "Effect of dispersion fluctuations on widely tunable optical parametric amplification in photonic crystal fibers," Opt. Express **14**(20), 9491–9501 (2006).
7. M. E. Marhic, N. Kagi, T. K. Chiang, and L. G. Kazovsky, "Broadband fiber optical parametric amplifiers," Opt. Lett. **21**(8), 573–575 (1996).
8. J. M. Chavez Boggio, S. Tenenbaum, and H. L. Fragnito, "Amplification of broadband noise pumped by two lasers in optical fibers," J. Opt. Soc. Am. B **18**(10), 1428–1435 (2001).
9. C. Floridia, M. L. Sundheimer, L. S. Menezes, and A. S. L. Gomes, "Optimization of spectrally flat and broadband single-pump fiber optic parametric amplifiers," Opt. Commun. **223**(4-6), 381–388 (2003).
10. J. M. Chavez Boggio, J. D. Marconi, and H. L. Fragnito, "Double-pumped fiber optical parametric amplifier with flat gain over 47-nm bandwidth using a conventional dispersion-shifted fiber," IEEE Photonics Technol. Lett. **17**(9), 1842–1844 (2005).
11. P. Dainese, G. S. Wiederhecker, A. A. Rieznik, H. L. Fragnito, and H. E. Hernandez-Figueroa, "Designing fiber dispersion for broadband parametric amplifiers," *IEEE-SBMO, International Microwave and Optoelectronics Conference (IMOC)*, 2005, pp. 1–3.
12. J. M. Chavez Boggio, J. D. Marconi, S. R. Bickham, and H. L. Fragnito, "Spectrally flat and broadband double-pumped fiber optical parametric amplifiers," Opt. Express **15**(9), 5288–5309 (2007).
13. S. Pitois and G. Millot, "Experimental observation of a new modulational instability spectral window induced by fourth-order dispersion in a normally dispersive single-mode optical fiber," Opt. Commun. **226**(1-6), 415–422 (2003).
14. J. Harvey, R. Leonhardt, S. Coen, G. Wong, J. Knight, W. Wadsworth, and P. S. J. Russell, "Scalar modulation instability in the normal dispersion regime by use of a photonic crystal fiber," Opt. Lett. **28**(22), 2225–2227 (2003).
15. M. E. Marhic, K. K.-Y. Wong, and L. G. Kazovsky, "Wide-band tuning of the gain spectra of one-pump fiber optical parametric amplifiers," IEEE J. Sel. Top. Quantum Electron. **10**(5), 1133–1141 (2004).
16. A. Y. H. Chen, G. K. L. Wong, S. G. Murdoch, R. Leonhardt, J. D. Harvey, J. C. Knight, W. J. Wadsworth, and P. S. J. Russell, "Widely tunable optical parametric generation in a photonic crystal fiber," Opt. Lett. **30**(7), 762–764 (2005).
17. W. H. Reeves, D. V. Skryabin, F. Biancalana, J. C. Knight, P. S. J. Russell, F. G. Omenetto, A. Efimov, and A. J. Taylor, "Transformation and control of ultra-short pulses in dispersion-engineered photonic crystal fibres," Nature **424**(6948), 511–515 (2003).
18. P. K. A. Wai, C. R. Menyuk, H. H. Chen, and Y. C. Lee, "Soliton at the zero-group-dispersion wavelength of a single-mode fiber," Opt. Lett. **12**(8), 628–630 (1987).
19. N. Akhmediev and M. Karlsson, "Cherenkov radiation emitted by solitons in optical fibers," Phys. Rev. A **51**(3), 2602–2607 (1995).
20. G. P. Agrawal, *Nonlinear Fiber Optics*, 5th ed. (Academic, 2013).
21. J. M. Dudley and J. R. Taylor, *Supercontinuum Generation in Optical Fibers* (Cambridge University, 2010).
22. A. Blanco-Redondo, C. M. de Sterke, J. E. Sipe, T. F. Krauss, B. J. Eggleton, and C. Husko, "Pure-quartic solitons," Nat. Commun. **7**(1), 10427 (2016).
23. M. Nakazawa, T. Yamamoto, and K. R. Tamura, "1.28 Tbit/s-70 km OTDM transmission using third- and fourth-order simultaneous dispersion compensation with a phase modulator," Electron. Lett. **36**(24), 2027–2029 (2000).
24. J. Capmany, D. Pastor, S. Sales, and B. Ortega, "Effects of fourth-order dispersion in very high-speed optical time-division multiplexed transmission," Opt. Lett. **27**(11), 960–962 (2002).

Optics EXPRESS

25. L. Zong, F. Luo, Y. Wang, and X. Cao, "Dispersion compensation module for 100 Gbit/s optical system and beyond," Opt. Fiber Technol. **17**(3), 227–232 (2011).
26. C. Mazzali, D. F. Grosz, and H. L. Fragnito, "Simple method for measuring dispersion and nonlinear coefficient near the zero-dispersion wavelength of optical fibers," IEEE Photonics Technol. Lett. **11**(2), 251–253 (1999).
27. H. Chen, "Simultaneous measurements of non-linear coefficient, zero-dispersion wavelength and chromatic dispersion in dispersion-shifted fibers by four-wave mixing," Opt. Commun. **220**(4-6), 331–335 (2003).
28. G. K. L. Wong, A. Chen, S. Ha, R. Kruhlak, S. Murdoch, R. Leonhardt, J. Harvey, and N. Joly, "Characterization of chromatic dispersion in photonic crystal fibers using scalar modulation instability," Opt. Express **13**(21), 8662–8670 (2005).
29. J. Fatome, S. Pitois, and G. Millot, "Measurement of nonlinear and chromatic dispersion parameters of optical fibers using modulation instability," Opt. Fiber Technol. **12**(3), 243–250 (2006).
30. B. Auguie, A. Mussot, A. Boucon, E. Lantz, and T. Sylvestre, "Ultralow chromatic dispersion measurement of optical fibers with a tunable fiber laser," IEEE Photonics Technol. Lett. **18**(17), 1825–1827 (2006).
31. J. M. C. Boggio and H. L. Fragnito, "Simple four-wave-mixing-based method for measuring the ratio between the third- and fourth-order dispersion in optical fibers," J. Opt. Soc. Am. B **24**(9), 2046–2054 (2007).
32. A. Gil-Molina, A. Perez-Ramirez, J. C. Ramirez, L. H. Gabrielli, and H. L. Fragnito, "Shift of zero-dispersion wavelength in bent optical fibers," Opt. Express **26**(6), 6700–6714 (2018).
33. M. Droques, B. Barviau, A. Kudlinski, G. Bouwmans, and A. Mussot, "Simple method for measuring the zero-dispersion wavelength in optical fibers," IEEE Photonics Technol. Lett. **23**(10), 609–611 (2011).
34. H. Onaka, K. Otsuka, H. Miyata, and T. Chikama, "Measuring the longitudinal distribuition of four-wave-mixing efficiency in dispersion-shifted fibers," IEEE Photonics Technol. Lett. **6**(12), 1454–1456 (1994).
35. I. Brener, P. P. Mitra, D. D. Lee, and D. J. Thomson, "High-resolution zero-dispersion wavelength mapping in single-mode fiber," Opt. Lett. **23**(19), 1520–1522 (1998).
36. M. Gonzalez-Herráez, P. Corredera, M. L. Hernanz, and J. A. Méndez, "Retrieval of the zero-dispersion wavelength map of an optical fiber from measurement of its continuous wave four-wave mixing efficiency," Opt. Lett. **27**(17), 1546–1548 (2002).
37. A. Mussot, E. Lantz, A. Durecu-Legrand, C. Simonneau, D. Bayart, T. Sylvestre, and H. Maillotte, "Zero-dispersion wavelength mapping in short single-mode optical fibers using parametric amplification," IEEE Photonics Technol. Lett. **18**(1), 22–24 (2006).
38. R. M. Jopson, M. Eiselt, R. H. Stolen, R. M. Derosier, A. M. Vengsarkar, and U. Koren, "Non-destructive dispersion-zero measurements along an optical fibre," Electron. Lett. **31**(24), 2115–2117 (1995).
39. M. Eiselt, R. M. Jopson, and R. H. Stolen, "'Nondestructive position-resolved measurement of the zero-dipersion wavelength in an optical fiber,'," J. Lightwave Technol. **15**(1), 135–143 (1997).
40. S. Nishi and M. Saruwatari, "'Technique for measuring the distributed zero dispersion wavelength of optical fibers using pulse amplification caused by modulation instability,'," Electron. Lett. **31**(3), 225–226 (1995).
41. L. F. Mollenauer, P. V. Mamyshev, and M. J. Neubelt, "Method for facile and accurate measurement of optical fiber dispersion maps," Opt. Lett. **21**(21), 1724–1726 (1996).
42. K.-Y. Song, M. González Herráez, and L. Thévenaz, "Mapping of chromatic-dispersion distribution along optical fibers with 20-m spatial resolution," J. Lightwave Technol. **23**(12), 4140–4146 (2005).
43. E. Myslivets, N. Alic, J. R. Windmiller, and S. Radic, "A new class of high-resolution measurements of arbitrary-dispersion fibers: localization of four-photon mixing process," J. Lightwave Technol. **27**(3), 364–375 (2009).
44. J. M. C. Boggio, S. Tenenbaum, J.D. Marconi, and H.L. Fragnito, "A novel method for measuring longitudinal variations of the zero dispersion wavelength in optical fibers," in *Proc. European Conference on Optical Communication (ECOC)*, September 2006, Cannes, France, paper Th1.5.2.
45. L. H. Gabrielli, H. E. Hernández-Figueroa, and H. L. Fragnito, "Robustness optimization of fiber index profiles for optical parametric amplifiers," J. Lightwave Technol. **27**(24), 5571–5579 (2009).
46. J. W. Goodman, *Statistical Optics*, 2nd ed. (John Wiley & Sons, 2015).
47. L. Mandel and E. Wolf, *Optical Coherence and Quantum Optics*, (Cambridge University, 1995).
48. A. Gil-Molina, I. A. Aldaya, and H. L. Fragnito, "Characterization of Fast Dispersion Fluctuations in Optical Fibers Using Incoherently Pumped Four-Wave Mixing," *Latin America Optics and Photonics Conference (LAOP)*, 2016, LTh3B-5.
49. K. C. Byron, M. A. Bedgood, A. Finney, C. McGauran, S. Savory, and I. Watson, "Shifts in zero dispersion wavelength due to pressure, temperature and strain in dispersion shifted singlemode fibres," Electron. Lett. **28**(18), 1712–1714 (1992).
50. A. A. Rieznik, T. Tolisano, F. A. Callegari, D. F. Grosz, and H. L. Fragnito, "Uncertainty relation for the optimization of optical-fiber transmission systems simulations," Opt. Express **13**(10), 3822–3834 (2005).
51. J. W. Fleming, "Dispersion in GeO2-SiO2 glasses," Appl. Opt. **23**(24), 4486–4496 (1984).
52. S. H. Wemple, D. A. Pinnow, T. C. Rich, R. E. Jaeger, and L. G. Van Uitert, "Binary SiO2-B2O3 glass system: Refractive index behavior and energy gap considerations," J. Appl. Phys. **44**(12), 5432–5437 (1973).
53. B. P.-P. Kuo, J. M. Fini, L. Grüner-Nielsen, and S. Radic, "Dispersion-stabilized highly-nonlinear fiber for wide band parametric mixer synthesis," Opt. Express **20**(17), 18611–18619 (2012).
54. A. Mussot, A. Kudlinski, R. Habert, I. Dahman, G. Mlin, L. Galkovsky, A. Fleureau, S. Lempereur, L. Lago, D. Bigourd, T. Sylvestre, M. W. Lee, and E. Hugonnot, "20 THz-bandwidth continuous-wave fiber optical parametric amplifier operating at 1 μm using a dispersion-stabilized photonic crystal fiber," Opt. Express **20**(27), 28906–28911 (2012).